Biosensors and Bioelectronics 131 (2019) 193–199

Contents lists available at ScienceDirect

Biosensors and Bioelectronics

journal homepage: www.elsevier.com/locate/bios

Ultrasensitive DNA biosensor based on electrochemical atom transfer radical polymerization

Haobo Sun[a,b,1], Yunliang Qiu[c,1], Qianrui Liu[b], Qiangwei Wang[b], Yan Huang[a], Dongxiao Wen[b], Xueji Zhang[d], Qingyun Liu[e,*], Guodong Liu[a,*], Jinming Kong[a,b,**]

[a] Research Center for Biomedical and Health Science, Anhui Science and Technology University, Fengyang 233100, PR China
[b] School of Environmental and Biological Engineering, Nanjing University of Science and Technology, Nanjing 210094, PR China
[c] Department of Criminal Science and Technology, Nanjing Forest Police College, Nanjing 210023, PR China
[d] Chemistry Department, College of Arts and Sciences, University of South Florida, East Fowler Avenue, Tampa, FL 33620-4202, United States
[e] College of Chemical and Environmental Engineering, Shandong University of Science and Technology, Qingdao 266590, PR China

ARTICLE INFO

Keywords:
DNA
Signal amplification
Electrochemical biosensor
Click reaction
SI-eATRP

ABSTRACT

Here we report a highly selective and ultrasensitive DNA biosensor based on electrochemical atom transfer radical polymerization (ATRP) signal amplification and "Click Chemistry". The DNA biosensor was prepared by immobilizing thiol and azide modified hairpin DNAs on gold electrode surface. In the presence of target DNAs (T-DNA), hairpin probes hybridized with T-DNAs to form a duplex DNA, and the ring of hairpin DNA was opened to make azide groups accessible at 3′ ends. "Click reactions" proceeded between the azide and propargyl-2-bromoisobutyrate (PBIB) to initiate the ATRP reaction which brought a large number of ferrocenylmethyl methacrylate (FMMA) on the electrode surface. The amount of FMMA was proportional to the concentration of T-DNA and quantified by square wave voltammetry. Combining ATRP signal amplification with "Click Chemistry", the optimized DNA biosensor was capable of detecting 0.2 aM. T-DNA. The preliminary application of the developed DNA biosensor was demonstrated by detecting target DNA in spiked serum samples. The developed DNA biosensor shows great promise for the detection of gene biomarkers.

1. Introduction

The nucleic acid test with high sensitivity and specificity is very important of central importance, especially in the field of diseases (Fan et al., 2006; Farjami et al., 2011), molecular diagnosis (Zhou et al., 2014), biomedical research (Palecek et al., 2012), medicine exploitation (Meng et al., 2016; Zhu et al., 2013), environmental monitoring (Zhou et al., 2017) and food safety (Li et al., 2010). Various strategies and technologies have been developed to identify unique DNA sequences. Agarose, and polyacrylamide gel electrophoresis (Southern, 1975; Zhu et al., 2015), real-time polymerase chain reaction (RT-PCR) (Doi et al., 2015), DNA microarrays (gene chip) (Cho and Tiedje, 2002), the surface Plasmon resonance BIAcore instrument (Ding et al., 2017) and GeneXpert system (Jones et al., 2001) have been used as standard procedures in research laboratories. Such conventional methods are generally laborious and time-consuming, requiring expensive instruments and highly trained personnel. Nucleic acid biosensors, in particularly, electrochemical DNA biosensors, have evolved dramatically over the past two decades and offer an alternative tool to overcome the above drawbacks. Compared with the other types of DNA biosensors, such as fluorescent DNA biosensor (Zhao et al., 2012), colorimetric DNA biosensor (Liu et al., 2013), and so on, electrochemical DNA biosensors received considerable attention in the field of biochemical analysis and medical research for its merits of simple operation, good selectivity, high sensitivity, miniaturation, low-cost and portability. Although existing electrochemical DNA biosensors have been developed in many aspects from the perspective of clinical application, there are still some defects such as poor stability, lacking detection sensitivity, poor specificity of capture probe, complex preparation process and long testing cycle.

The sensitivities of electrochemical DNA sensors have been enhanced dramatically by the use of novel signal amplification strategies (Qian et al., 2015a, 2015b, 2015c; Ren et al., 2015; Liu et al., 2017). Enzymes (Wang et al., 2011; Wang et al., 2014), nanomaterials

* Corresponding authors.
** Corresponding author at: Research Center for Biomedical and Health Science, Anhui Science and Technology University, Fengyang 233100, PR China.
E-mail addresses: qyliu@sdust.edu.cn (Q. Liu), liugd@ahstu.edu.cn (G. Liu), kong@njust.edu.cn (J. Kong).
[1] These authors contributed equally to this work.

https://doi.org/10.1016/j.bios.2018.11.029
Received 29 August 2018; Received in revised form 31 October 2018; Accepted 18 November 2018
Available online 19 November 2018
0956-5663/

Table 1
The detailed sequences of oligonucleotides.

Note	Sequence (5′-3′)
Hairpin probe (cDNA)	SH-$(CH_2)_6$-CCA CGC TTG TGG GTC AAC CCC CGT GG-N_3
Complementary target ssDNA (T-DNA)	GGG GTT GAC CCA CAA G
Single -base mismatched ssDNA (Sm-DNA)	GGG GTCGAC CCA CAA G
Three-bases mismatched ssDNA (Tm-DNA)	GGG GTCGTC GCA CAA G
Non-complementary DNA (N-DNA)	TTC AGC TCT ATC AAT C

(Samanta and Medintz, 2016; Loan et al., 2014) and electrochemical active substance (Qian et al., 2015a, 2015b, 2015c) were used as labels to improve the detection limits of electrochemical DNA biosensors. Combining nucleic acid amplification approaches including isothermal amplification, (Reid et al., 2018), strand displacement amplification, (Walker et al., 1992) exonuclease III auxiliary signal amplification (Gao and Li, 2014) and rolling circle amplification (Xiong et al., 2015, 2014) with sensitive electrochemical detection, the detection limits of electrochemical DNA detection were improved dramatically. However, complex process, high-cost and easy-contamination prevent their use in research laboratories and practical applications. Therefore, it is very urgent for developing a compendious method for ultrasensitive DNA detection.

Here, we report a novel DNA detection method based on electrochemically mediated surface-initiated atom transfer radical polymerization (SI-eATRP) and click chemistry. ATRP uses simple organic halides as initiators and metal complex as halogen atom carrier., A reversible dynamic equilibrium between active species and dormant species was established. ATRP could control the polyreactions (Matyjaszewski and Xia, 2001; Magenau et al., 2011; Wang and Matyjaszewski, 1995a, 1995b). This method was firstly reported by Wang and Matyjaszewski in 1995, featuring in many kinds of monomers and synthesis of gradient copolymer and industrial polymerization (Wang and Matyjaszewski, 1995a, 1995b). In this work, we report an electrochemical DNA detection approach with high sensitivity and selectivity by utilizing SI-eATRP and “click chemistry” (Díaz et al., 2004; El-Sagheer and Brown, 2010). The selectivity of the method has been greatly improved by using hairpin as a capture probe, which makes it applicable for analysis of single nucleotide polymorphisms (SNPs). Electrochemically mediated polymerization results in the accumulation of a large number of electroactive probes on the surface of the electrode, which remarkably improved the sensitivity of electrochemical detection. In addition, this "signal-on" approach can avoid the interference of false positive results. Compared to other signal amplification strategies that use existing polymer materials directly, electrochemically mediated polymerization has the characteristics of simple and efficient, which can significantly improve the coupling rate and efficiency of polymer. Results show that this method is suitable for SNPs analysis, and it has strong anti-interference ability for ssDNA analysis in serum samples. On the proposed signal amplification strategy can be applied for the detection of other biological molecules.

2. Experimental

2.1. Chemicals and reagents

All chemicals and reagents were analytical grade or higher, and used as received without further purification. Ultrapure water was used in all experiments. Sodium borohydride ($NaBH_4$), bathophenanthrolinedisulfonic acid disodium salt hydrate (BPDS), propargyl-2-bromoisobutyrate (PBIB), copper (II) sulfate ($CuSO_4$), ferrocenylmethyl methacrylate (FMMA) and 6-mercapto-1-hexanol (MCH) were purchased from Sigma-Aldrich (St. Louis, USA). Ascorbic acid (AA), potassium bromide (KBr), potassium hexafluorophosphate (KPF_6), copper (II) bromide ($CuBr_2$), ethynylferrocene (EFC), lithium perchlorate trihydrate ($LiClO_4$) and tris(2-dimethylaminoethyl)amine (Me_6TREN) were purchased from J&K Scientific Ltd. (Shanghai, China). N, N-Dimethylformamide (DMF), hydrochloric acid (HCl), sulfuric acid (H_2SO_4), ethanol absolute and other chemicals were ordered from Sinopharm Chemical Reagent Co., Ltd. (Shanghai, China). Normal human serum (NHS) was obtained from Shanghai YiJi Industrial Co., Ltd. (Shanghai, China).

All oligonucleotides were synthesized by Shanghai Shenggong Biotechnology Co. (Shanghai, China) with purity no less than 99%. The oligonucleotide stock solutions were prepared with Tris-EDTA buffer (TE, 10 mM Tris-HCl, 1 mM EDTA, pH = 7.6) and kept frozen. The hairpin DNA solution was prepared and diluted with TE buffer containing 100 mM $MgCl_2$ (pH 7.6). The sequences of oligonucleotides were described below (Table 1):

2.2. Pretreatment of gold electrode

Bare gold electrodes were polished with 0.3 and 0.05 μm alumina suspensions respectively, and then sequentially washed ultrasonically in 99.99% ethanol and ultrapure water. After that, the bare gold electrode was soaked in freshly prepared piranha solution (30% H_2O_2 and 98% H_2SO_4, 1:3 v/v) for 10 min. Subsequently electrochemical clean process was proceeded by the potential scanning between −0.2 and 1.5 V until a reproducible cyclic voltammogram (CV) was formed in 0.5 M H_2SO_4 (Hu et al., 2015). Finally, the electrode was rinsed with ultrapure water, then dried with high purity nitrogen and then used.

2.3. Self-assembling hairpin DNA on gold electrode

Hairpin DNA was dissolved in TE buffer (10 mM Tris-HCl, 1 mM EDTA, pH = 7.4). At the temperature of 37 °C, 5 μL of thiolated hairpin DNA (0.5 μM) was dropped on the surface of the cleaned gold electrode. After 1.5 h, the electrode was washed twice with TE buffer. During this process, the hairpin DNA was immobilized on the surface of the gold electrode through the Au-S bond. Followed by a 0.5 h blocking with an aqueous solution of 2.0 mM MCH (dissolved in 70% ethanol), the electrode was washed with TE buffer before further treatment. Hybridization reactions between the hairpin DNA and T-DNA proceeded 1.5 h at 37 °C by dropping 10.0 μL T-DNA onto the gold electrode surface. TE buffer was used to wash the electrode surface and wipe off the unbound oligonucleotides.

Unfolded hairpin probes on the gold electrode surface were then labeled with PBIB through the copper-catalyzed azide-alkyne cycloaddition (CuAAC). The “click reaction” was carried out in 400 μL of solution (0.1 mM PBIB 0.1 mM $CuSO_4$ and 0.2 mM AA) at 25 °C for 0.5 h. Then the gold electrode was washed with TE buffer for 10 s.

Afterwards, an electrochemical-based ATRP macromolecular initiation process proceeded between the attached PBIB and FMMA via CuI-catalyzed reaction: eATRP of FMMA was carried out in the electrolytic cell containing labeling solution ([FMMA]: [Cu^{II}/Me_6TREN]: [KBr]: [DMF]: [KPF_6] = 1:1:10:18:70 v/v). After labeling was completed, the electrode was subject to linear sweep voltammetry (LSV) (initial potential: 0 V; final potential: 0.2 V; scan rate: 1.0 Vs^{-1}). Finally, physically adsorbed Cu° and FMMA were eliminated via cleaning with DMF and ultrapure water.

2.4. Electrochemical measurement

The square wave voltammetry (SWV) was used to measure the redox current of ferrocene in 1.0 M $LiClO_4$, and the range of potential scanning was from 0 V to 0.6 V with 4.0 mVs^{-1} of increase potential and 25 mV of the pulse amplitude.

2.5. Apparatus

All electrochemical measurements, including CV, LSV and SWV were performed at room temperature on a CHI 760D electrochemical workstation (chenghua, Shanghai. China). Reference electrode and the counter electrode were saturated calomel electrode (SCE) and platinum wire, respectively. Electrochemical impedance spectroscopy (EIS) was measured on Autolab/PGSTAT302N (Eco Chemie, Netherlands).

3. Results and discussion

3.1. The principle of electrochemical DNA biosensor

The principle of electrochemical DNA biosensor for the detection of DNA is depicted in Scheme 1. The biosensor was prepared by immobilizing the hairpin DNA probe that dually labeled with thiol at 5′ end and the azide group at 3′ end on the gold electrode surface through Au-thiol interaction followed by MCH blocking. After adding the T-DNA, the ring of hairpin DNA was opened and the azide group was liberated. Then the accessible azide group participated in "click reaction" process in the presence of initiator (PBIB), and CuAAC. Through redox reaction, Cu^{II} could be conveniently converted to Cu^{I}, which led to ATRP initiator (PBIB) attach to the electrode. Afterwards, numerous FMMA was captured on the electrode surface via eATRP. The success of ATRP process depends on a rapid and reversible activation/deactivation step. During the chain initiation phase of eATRP, Cu^{II}/Me_6TREN is reduced to Cu^{I}/Me_6TREN under constant voltage, which removes the Br atom from PBIB, generating deactivators (Cu^{II}Br/Me_6TREN) and propagating radicals (R•). Immediately after the chain growth stage, the radical R• initiates the polymerization of monomeric ferrocenylmethyl methacrylate (FMMA), and the Cu^{I}/Me_6TREN abstracts to Br atom from the polyferrocenylmethyl methacrylate (PFMMA), it then forms radical R-FMMA•. After that, chain radicals capture Br from the Cu^{II}Br/Me_6TREN and passivation reaction occurs, which means dormant macromolecular species (PFMMA-Br) are formed. Subsequently, PFMMA-Br works as a new initiator. The aforementioned ATRP reaction can be repeated, therefore the chain continues to grow, leading to multiple FMMA connected to DNA duplex. Eventually the amount of FMMA on the electrode surface was quantified by SWV, generating an enhanced current signal. The SWV response of FMMA depends on the T-DNA concentration and can be used for DNA quantitative detection.

3.2. Feasibility of the biosensor

A constant potential (E_{app})was used to reduce Cu^{II}Br/Me_6TREN to Cu^{I}/ Me_6TREN. (Devaraj et al., 2006). In this study, the E_{app} was determined by CV with the potential range of −0.8–0.5 V and scanning rate of 0.1 $V s^{-1}$ in FMMA-free eATRP cocktail solution. As shown in Fig. 1**A**, anodic peak "A_p" represents Cu^{II}, cathode peak "C_p" represents that Cu^{II} was reduced to Cu^{I}, and Cu^{II}Br/Me_6TREN was reduced to Cu^{I}/ Me_6TREN at the potential of −0.55 V vs SCE. When E_{app} is more positive, polymerization would become easier, but the reaction rate will be reduced. At a more negative potential, more Cu^{I}/Me_6TREN would be obtained, and in this case, the reaction rate was too fast, which led to the deterioration of the polymerization. Therefore SI-eATRP was performed at −0.55 V vs. SCE. The selectivity of Cu^{+} in the ATRP reaction against other metal ions such as $Cu^{2+}$and Ni^{2+} was studied. It was found that there was no current response obtained without applying a constant potential or in the presence of Ni^{2+}, indicating Cu^{+} has excellent catalytic performance. The result is consistent with that reported in the literature (Magenau et al., 2011).

In order to demonstrate the feasibility of the proposed signal amplification strategy for T-DNA detection, we compared the SWV responses of the electrodes, which were prepared step-by-step during the SI-eATRP process. Fig. 1**B** shows the SWV responses of the electrodes. There was no current observed with both bare gold electrode (**curve a**) and hairpin DNA/MCH/PBIB/FMMA-modified gold electrode (the electrode was prepared in the absence of the T-DNA, **curve b**), indicating that no FMMA was attached on the electrode surface. An oxidation current was observed with hairpin DNA/MCH/tDNA/EFC-modified gold electrode (**curve c)**, which was prepared in the presence of 10 fM of T-DNA. In this case, the loop of hairpin DNA probe was opened due to the hybridization reactions between T-DNA and hairpin DNA and initiated the "click reaction". EFC was then attached to the electrode surface. The oxidation current was derived from the electrochemical oxidation of ferrocene in ferrocenium cation. Following ATRP reaction, the SWV response was enhanced dramatically with Hairpin DNA/MCH/tDNA/PBIB/FMMA-gold electrode (**curve d)**. Such significant signal amplification would be ascribed to the ATRP reaction, which brought a large amount of FMMA to the electrode surface.

Moreover, the hairpin DNA/MCH/tDNA/PBIB/FMMA-gold

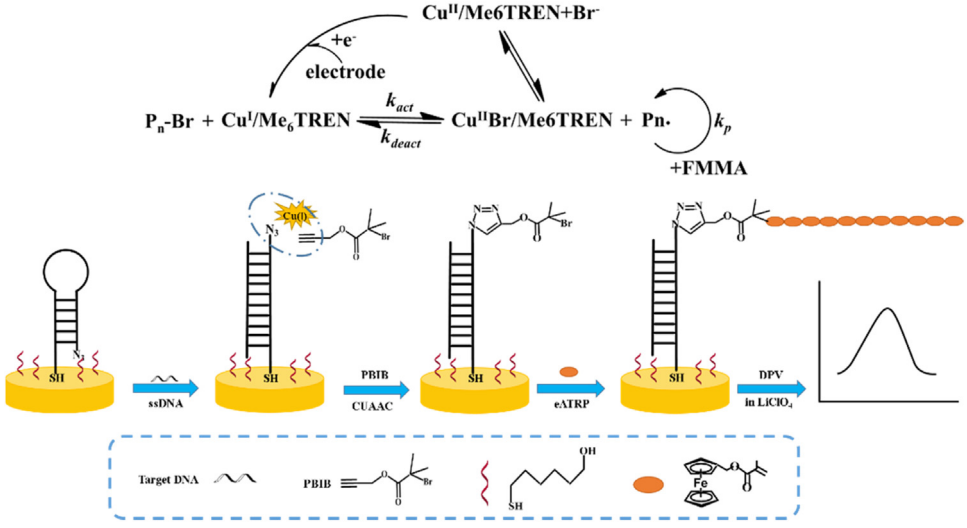

Scheme 1. Schematic illustration of the principle of electrochemical DNA biosensor based on click chemistry and ATRP. See details in the text and supplement.

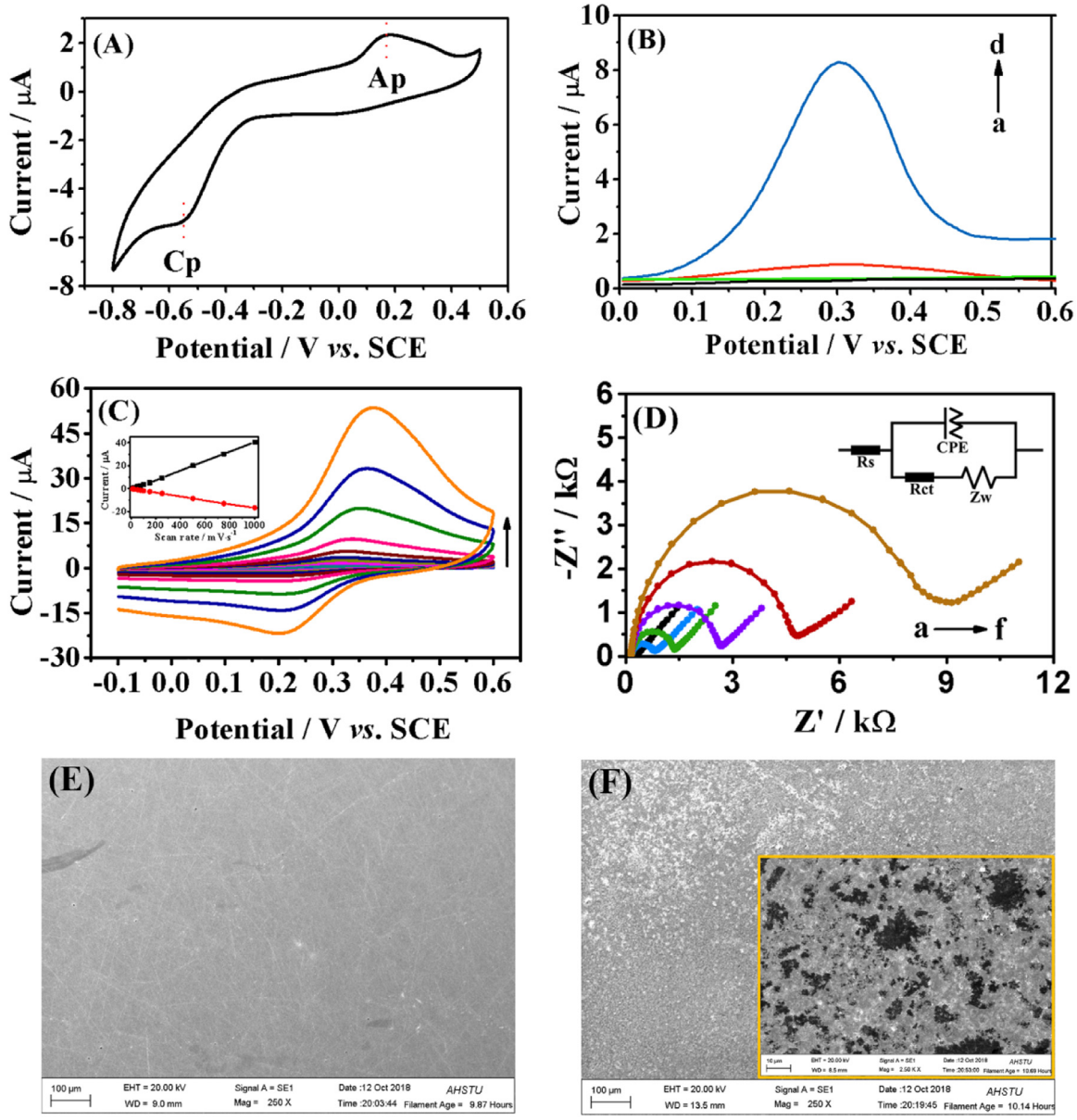

Fig. 1. (A) CVs of the hairpin DNA /MCH/tDNA/PBIB -modified gold electrodes in the FMMA-free eATRP mixture. The concentration of tDNA was 10 fM. Scan rate: 0.1 V s^{-1}. (B) SWV curves of bare gold electrode(a), hairpin DNA/MCH/PBIB/FMMAgold electrode (b), hairpin DNA/MCH/tDNA/EFCgold electrode(c), and hairpin DNA/MCH/tDNA/PBIB/FMMA-gold electrode (d) in $LiClO_4$. (C) the CVs of hairpin DNA/MCH/tDNA/PBIB/FMMA modified gold electrode at different scan rate ranging from 10 to 1000 mV s^{-1}. Inset: The relationship between oxidation (black line) and reduction (red line) peak currents and scan rates in 1.0 M $LiClO_4$; (D)The Nyquist plots of the bare gold electrode (a), hairpin DNA modified gold electrode (b), hairpin DNA/MCH modified gold electrode (c), hairpin DNA/MCH/tDNA modified gold electrode (d), hairpin DNA/MCH/tDNA/PBIB modified gold electrode (e) and hairpin DNA/MCH/tDNA/PBIB/FMMA modified gold electrode (f). EISs were obtained in 0.1 M KNO_3 aqueous solution containing 5 mM $K_3[Fe(CN)_6]/K_4[Fe(CN)_6]$. (E) The SEM image of hairpin DNA/MCH/tDNA/PBIB/gold electrode. (F) The SEM image of the polymer-grafted gold electrode (hairpin DNA/MCH/tDNA/PBIB/FMMA modified gold electrode). Inset is the SEM image of the polymer-grafted gold electrode with high resolution.

electrode was further characterized by CV at different scanning rates. One can see that the differences of peak potential between the oxidation peak and the reduction peak gradually increases with the increase of the scanning rates (Fig. 1**C**), indicating the redox process of ferrocene is a quasi-reversible process. It is noted that the peak current increases with the scanning speed increasing. **Inset of** Fig. 1**C** shows the relationship between the peak current and the potential scanning speed. Both the oxidation peak current and reduction peak current are proportional to the potential scanning speed, which is consistent with the previous report (Chang et al., 2010). It indicates the redox process of ferrocene is mainly kinetic control and is an adsorption process that takes place on the electrode surface. It was once again demonstrated that FMMA was successfully attached on the electrode surface by "click chemistry" and ATRP reaction.

3.3. Characterization of the biosensor

SWV and EIS were used to study the interface properties of the biosensor corresponding to the stepwise modification processes. In a typical EIS measurement, the EIS curves (Fig. 1**D**) were obtained in 0.1 M KNO_3 containing 5 mM $[Fe(CN)_6]^{3-}/[Fe(CN)_6]^{4-}$. Generally, the EIS results can be considered as equivalent circuits (**inset,** Fig. 1**D**) which include the electrolyte solution resistance R_s, the constant phase element (CPE), the surface electron transfer resistance R_{ct}, the diffusion

resistance R_w and the Warburg impedance Z_w. The diameter of semicircle was equivalent to the electron transfer resistance (R_{ct}) in the Nyquist plot of impedance spectroscopy. One can see the EIS of the pretreated bare gold electrode shows a very small semicircle domain (R_{ct} = 0.15 kΩ, **curve a**) in 0.1 M KNO_3 containing 5 mM $[Fe(CN)_6]^{3-}$/$[Fe(CN)_6]^{4-}$, indicating the electroactive ions were rapidly transported to the electrode interface. A large semicircle with Rct value of approximately 0.70 kΩ (**curve b**) was obtained with the hairpin DNA probe modified gold electrode. Such increase of Rct value could be contributed by the negative charge of the phosphate backbone of the hairpin DNA, thereby repelling the anion $[Fe(CN)_6]^{3-}$/$[Fe(CN)_6]^{4-}$ diffusion to the electrode surface. Subsequently, the electrode blocked with MCH resulted in a further increase of R_{ct} (R_{ct} = 1.32 kΩ, **curve c**). It is noted that the hybridization of T-DNA with the hairpin probe on the gold electrode surface resulted in a large increase in R_{ct} (R_{ct} = 2.50 kΩ, **curve d**), probably due to the formation of the hairpin-target DNA duplexes and further limited the diffusion of $[Fe(CN)_6]^{3-}$/$[Fe(CN)_6]^{4-}$ to the surface of the gold electrode. When the PBIB was introduced to the electrode surface by "click reaction", the R_{ct} increased (R_{ct} = 4.63 kΩ, **curve e**) again, which was attributed to the ATRP initiator that could prevent the electron transfer. After the ATRP reaction completed, the R_{ct} was raised to 8.70 kΩ (curve f). This can be illustrated by the accumulation of a large amount of FMMA on the electrode surface and hindering the electron transfer of $[Fe(CN)_6]^{3-}$/$[Fe(CN)_6]^{4-}$. SEM was used to characterize the appearance of hairpin DNA/ MCH/ tDNA/ PBIB/ gold electrode prior to and after ATRP reaction. As shown in Fig. 1(E), no material was observed on the electrode surface before the ATRP reaction. After the ATRP reaction, one can see that the electrode surface shows high-density mountainous protrusions, confirming the formation of the polymer (Fig. 1**(F)**). Inset in Fig. 1 **(F)** is the SEM image of the electrode surface with high resolution. The above results manifest that all steps shown in Scheme 1 were successfully executed.

3.4. Optimization of experimental conditions

To achieve the best performance of the biosensor, experimental parameters including the concentration of the hairpin DNA probe used for self-assembling, the self-assembling time, hybridization reaction time, "click reaction" time and ATRP time were studied. As shown in Fig. S-2A, the peak current increased with the increase of hairpin DNA probe concentration and tended to decrease at 0.6 μM. The decrease of peak current at higher concentrations of hairpin DNA probe could be caused by steric hindrances, which prevented the DNA probe to form the hairpin structures. Therefore, the concentration of DNA probe used in the subsequent experiments was 0.6 μM. The self-assembling time of DNA probe on the gold electrode was explored from 15 min to 120 min. As shown in Fig. S-2B, the peak current saturated after 90 min. So, 90 min was used as the optimum self-assembling time of DNA probe. The time of hybridization reaction between the hairpin DNA and T-DNA and the time of "click reaction" were also optimized (Fig. S-2**C-D**). It was found that the peak currents increased with the increase of both hybridization reaction time and click reaction time, and then tended to be saturated state. The optimal hybridization reaction and "click reaction" times of 90 min and 30 min were selected in the following experiment, respectively.

To further improve the sensitivity of the biosensor, the ATRP time was also optimized. Fig. 2A presents the effect of ATRP time on the SWV response of the biosensor. The peak current increased with the increment of incubating time and reached the maximum at 60 min (Fig. 2**B**). Thus 60 min was selected as the optimal ATRP reaction time.

3.5. Analytical performance

Under the optimal experimental conditions, the dynamic range and sensitivity of the proposed electrochemical DNA biosensor was evaluated by testing the sample solution containing different concentrations of T-DNA. As shown in Fig. 3**A,** the SWV peak current increased with the increase of the T-DNA concentration. As could be seen in Fig. 3**B**, there is a linear relationship between the peak current and the logarithm of the DNA concentration, which ranges from 10 aM to 10 pM The linear regression equation is $I = 4.83 + 0.76 \log [C_{tDNA}]$, and the correlation coefficient $R^2 = 0.995$, where I and C represent the peak current (μA) and the concentration of T-DNA (fM), respectively. The detection limit is estimated to be 0.2 a.M. (S/N = 3), which is lower than that of previously reported methods (Table S1).

Selectivity and reproducibility are two important parameters to evaluate a biosensor's performance. The specificity of the biosensor was assessed by testing the responses of T-DNA, Sm-DNA (single base-mismatched DNA), Tm-DNA (three bases-mismatched DNA) and N-DNA (noncomplementary DNA) at 10 fM. As illustrated in Fig. 4**A**, the peak current of the biosensor in the presence of T-DNA was 4.3-fold and 5.0-fold higher than that in the presence of Sm-DNA and Tm-DNA, respectively. A small peak current was obtained in the presence of N-DNA. Above results indicate the biosensor was able to differentiate T-DNA from Sm-DNA, Tm-DNA and N-DNA. Such excellent specificity for T-DNA would be ascribed to the hairpin DNA probe with a stem-loop conformation, which can distinguish mismatched and non-complementary DNA sequences (Fan et al., 2003). The selectivity against proteins coexisting in human plasma was studied by adding the proteins (albumin, globulins, fibrinogen and IgG) in the incubation buffer. Current change of the biosensor was neglectable in the presence and absence of plasma proteins.

The sensitive and specific response was coupled with high reproducibility. The reproducibility was studied by testing the sample solutions containing 10 pM. T-DNA. Samples from the same batch were

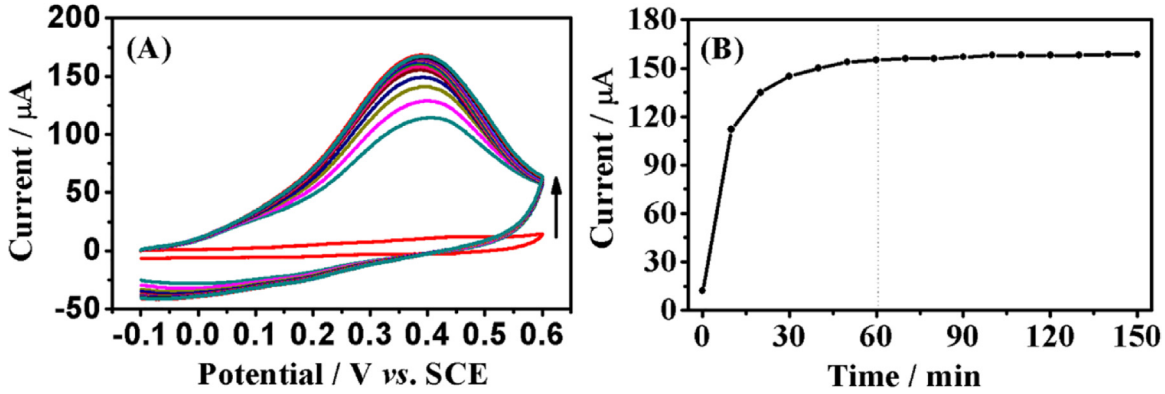

Fig. 2. Optimization of the experimental conditions. (A) CVs of hairpin DNA/MCH/tDNA/PBIB modified gold ectrode in eATRP mixture. Scans were taken every ten minutes. Scan rate: 1.0 V s^{-1}. The concentration of tDNA was 10 fM. (B) The plot of peak current versus eATRP time.

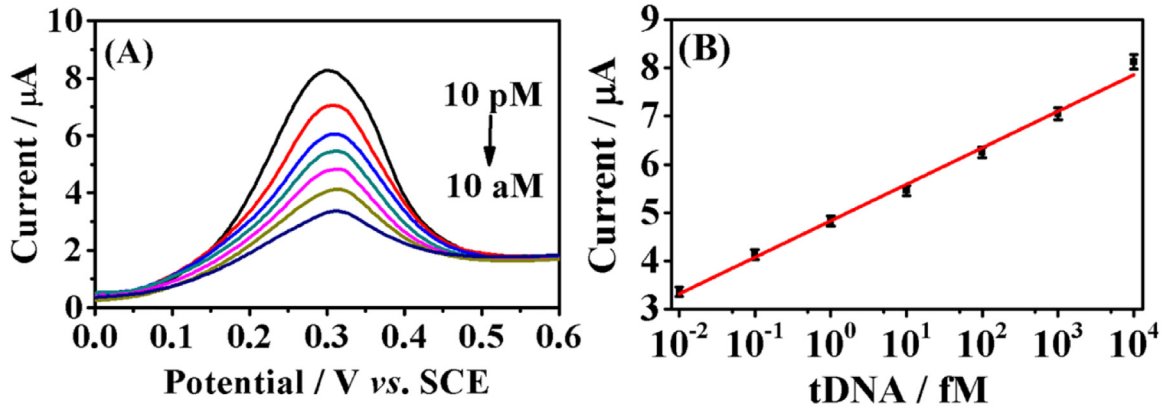

Fig. 3. (A) The SWV responses of the biosensor in the presence of different concentrations of T-DNA. The concentrations of T-DNA over the range of 10 aM to 10 fM. (B) Corresponding calibration curve. The error bars were obtained based on six repetitive experiments.

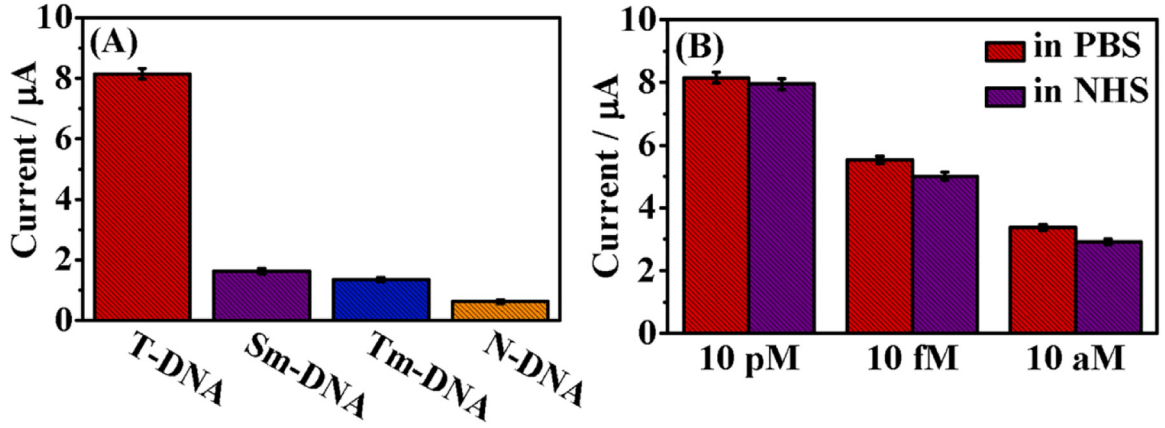

Fig. 4. (A) The histogram of SWV responses of the biosensor in the presence of T-DNA, single-base mismatched DNA (Sm-DNA), three-base mismatched DNA (Tm-DNA), and non-complementary DNA(N-DNA) at a concentration of 10 fM. (B) SWV responses of the biosensor in sample solutions prepared with PBS buffer and 5% diluted normal human serum. The concentrations T-DNA were 10 pM, 10 fM, 10 aM. Error bars were obtained on the basis of six replicate experiments.

tested 6 times with a single electrode. A relative standard deviation (RSD) of 2.6% was obtained. In addition, we prepared six electrodes under the same experimental conditions, and tested the responses of the biosensor in the presence of 10 pM. T-DNA. The RSD of SWV responses of the biosensors was 3.2%, showing good reproducibility.

The stability of the DNA biosensors was investigated by measuring its SWV responses after storing different periods at 4 °C. There was no obvious signal change observed after storing 30 days, demonstrating satisfactory stability.

3.6. Detection of DNA in spiked human serum

To demonstrate the feasibility of the proposed biosensor for biological application, the biosensor was then applied to detect T-DNA in spiked human serum. The sample solutions were prepared by adding 10 pM. T-DNA in 5% (v/v) diluted healthy human serum (NHS). As shown in Fig. 4**B**, for 10 pM., 10 fM and 10 aM. tDNA, SWV responses in 5% NHS samples were about 97.5%, 90.3%, and 86.4%, respectively, of the SWV response in PBS buffer. Since the unbound material in the real sample is removed by the TE buffer prior to click chemistry, the ions and proteins in the real sample will not interfere with subsequent click chemistry, ATRP reaction, and final detection. The result indicating that the DNA biosensor is feasible in real biological samples and has great clinical analysis potential.

4. Conclusions

We have developed a highly selective and ultrasensitive DNA biosensor using electrochemically mediated surface-initiated atom transfer radical polymerization (ATRP) signal amplification and “Click Chemistry”. Under optimal conditions, the biosensor was capable of detecting minimum 0.2 aM. target DNA. The preliminary application of the developed DNA biosensor was demonstrated by detecting target DNA in spiked serum samples. More optimizations are required to shorten the total assay time for real biosensor applications. The developed DNA biosensor shows great promise for the detection of gene biomarkers such as microRNA.

Acknowledgments

This work was financially supported by the National Natural Science Foundation of China (21575066) and the Wanjiang Scholars of Anhui Province, China.

Appendix A. Supplementary material

Supplementary data associated with this article can be found in the online version at doi:10.1016/j.bios.2018.11.029.

References

Cho, J.C., Tiedje, J.M., 2002. J. Appl. Environ. Microbiol. 68 (3), 1425–1430.
Chang, H., Tang, L., Wang, Y., Jiang, J., Li, J., 2010. Anal. Chem. 82 (6), 2341–2346.

Doi, H., Takahara, T., Minamoto, T., Matsuhashi, S., Uchii, K., Yamanaka, H., 2015. Environ. Sci. Technol. 49 (9), 5601–5608.
Ding, X., Cheng, W., Li, Y., Wu, J., Li, X., Cheng, Q., Ding, S., 2017. Biosens. Bioelectron. 87, 345–351.
Díaz, D.D., Punna, S., Holzer, P., McPherson, A.K., Sharpless, K.B., Fokin, V.V., Finn, M.G., 2004. J. Polym. Sci. A Polym. Chem. 42 (17), 4392–4403.
Devaraj, N.K., Dinolfo, P.H., Chidsey, C.E., Collman, J.P., 2006. J. Am. Chem. Soc. 128 (6), 1794–1795.
El-Sagheer, A.H., Brown, T., 2010. Chem. Soc. Rev. 39 (4), 1388–1405.
Fan, J.B., Chee, M.S., Gunderson, K.L., 2006. Nat. Rev. Genet. 7 (8), 632.
Farjami, E., Clima, L., Gothelf, K., Ferapontova, E.E., 2011. Anal. Chem. 83 (5), 1594–1602.
Fan, C., Plaxco, K.W., Heeger, A.J., 2003. Proc. Natl. Acad. Sci. USA 100 (16), 9134–9137.
Gao, Y., Li, B., 2014. Anal. Chem. 86 (17), 8881–8887.
Hu, Q., Deng, X., Yu, X., Kong, J., Zhang, X., 2015. Biosens. Bioelectron. 65, 71–77.
Jones, M., Alland, D., Marras, S., El-Hajj, H., Taylor, M.T., McMillan, W., 2001. Clin. Chem. 47 (10), 1917–1918.
Jiang, H.X., Kong, D.M., Shen, H.X., 2014. Biosens. Bioelectron. 55, 133–138.
Li, D., Song, S., Fan, C., 2010. Acc. Chem. Res. 43 (5), 631–641.
Liu, S., Fang, L., Tian, Y., Wei, W., Wang, L., 2017. Sens. Actuators B Chem. 244, 450–457.
Liu, P., Yang, X., Sun, S., Wang, Q., Wang, K., Huang, J., Liu, J., He, L., 2013. Anal. Chem. 85 (16), 7689–7695.
Loan, P.T.K., Zhang, W., Lin, C.T., Wei, K.H., Li, L.J., Chen, C.H., 2014. Adv. Mater. 26 (28), 4838–4844.
Meng, H.M., Liu, H., Kuai, H., Peng, R., Mo, L., Zhang, X.B., 2016. Chem. Soc. Rev. 45 (9), 2583–2602.
Matyjaszewski, K., Xia, J., 2001. Chem. Rev. 101 (9), 2921–2990.
Magenau, A.J., Strandwitz, N.C., Gennaro, A., Matyjaszewski, K., 2011. Science 332 (6025), 81–84.
Palecek, E., Bartosik, M., 2012. Chem. Rev. 112 (6), 3427–3481.
Qian, Y., Gao, F., Du, L., Zhang, Y., Tang, D., Yang, D., 2015a. Biosens. Bioelectron. 74, 483–490.
Qian, Y., Wang, C., Gao, F., 2015b. Biosens. Bioelectron. 63, 425–431.
Qian, Y., Tang, D., Du, L., Zhang, Y., Zhang, L., Gao, F., 2015c. Biosens. Bioelectron. 64, 177–181.
Ren, W., Gao, Z.F., Li, N.B., Luo, H.Q., 2015. Biosens. Bioelectron. 63, 153–158.
Reid, M.S., Le, X.C., Zhang, H., 2018. Angew. Chem. Int. Ed.
Southern, E.M., 1975. J. Mol. Biol. 98 (3), 503–517.
Samanta, A., Medintz, I.L., 2016. Nanoscale 8 (17), 9037–9095.
Wang, F., Elbaz, J., Orbach, R., Magen, N., Willner, I., 2011. J. Am. Chem. Soc. 133 (43), 17149–17151.
Wang, F., Lu, C.H., Willner, I., 2014. Chem. Rev. 114 (5), 2881–2941.
Walker, G.T., Little, M.C., Nadeau, J.G., Shank, D.D., 1992. Proc. Natl. Acad. Sci. 89 (1), 392–396.
Wang, J.S., Matyjaszewski, K., 1995a. Macromolecules 28 (23), 7901–7910.
Wang, J.S., Matyjaszewski, K., 1995b. J. Am. Chem. Soc. 117 (20), 5614–5615.
Xiong, E., Zhang, X., Liu, Y., Zhou, J., Yu, P., Li, X., Chen, J., 2015. Anal. Chem. 87 (14), 7291–7296.
Zhou, W., Huang, P.J.J., Ding, J., Liu, J., 2014. Analyst 139 (11), 2627–2640.
Zhu, G., Zheng, J., Song, E., Donovan, M., Zhang, K., Liu, C., Tan, W., 2013. Proc. Natl. Acad. Sci. USA 110 (20), 7998–8003.
Zhou, W., Saran, R., Liu, J., 2017. Chem. Rev. 117 (12), 8272–8325.
Zhu, X., Shi, H., Shen, Y., Zhang, B., Zhao, J., Li, G., 2015. Nano Res. 8 (8), 2714–2720.
Zhao, X.H., Ma, Q.J., Wu, X.X., Zhu, X., 2012. Anal. Chim. Acta 727, 67–70.